DOI: https://doi.org/10.2138/am-2020-7211

Revision 2

Metamorphic amphiboles in the Ironwood Iron-Formation, Gogebic Iron Range, Wisconsin: Implications for potential resource development

CARLIN J. GREEN[1], ROBERT R. SEAL II[1], NADINE M. PIATAK[1], WILLIAM F. CANNON[1], RYAN J. MCALEER[1], AND JULIA NORD[2]

[1]United States Geological Survey, 954 National Center, Reston, Virginia 20192, USA

[2]George Mason University, 4400 University Drive, Fairfax, VA 22030, USA

Abstract

The Paleoproterozoic Ironwood Iron-Formation, a Superior-type banded iron formation located in the western Gogebic Iron Range in Wisconsin, is one of the largest undeveloped iron ore resources in the United States. Interest in the development of this resource is complicated by potential environmental and health effects related to the presence of amphibole minerals in the Ironwood, a consequence of Mesoproterozoic contact metamorphism. The presence of these amphiboles and their contact metamorphic origin have long been recognized; however, recent interest in this resource has highlighted the lack of detailed knowledge on their distribution, mineral chemistry, and morphology. Optical microscopy, X-ray diffraction, scanning electron microscopy, and electron microprobe analysis were utilized to investigate the origin, distribution, morphology, and chemistry of amphiboles in the Ironwood.

Amphibole is present in the western portion of the study area due to regional-scale contact metamorphism associated with the intrusion of the 1.1 Ga Mellen Intrusive Complex.

Locally amphibole is also present adjacent to diabase and/or gabbro dikes and sills in the lower-grade Ironwood in the eastern portion of the study area. In both localities, amphiboles in the Ironwood most commonly developed in massive and prismatic habits, and locally assumed a fibrous habit. Fibrous amphiboles were recognized locally in the two potential ore zones of the Ironwood but were not observed in the portion likely to be waste rock. Massive and prismatic amphiboles show a wide range of Mg# (molar Mg/(Mg+Fe^{2+})) values (0.06 to 0.87), whereas Mg# values of fibrous amphiboles are restricted from 0.14 to 0.35. Factors that influenced the compositional variability of amphiboles in the Ironwood may have included temperature of formation, morphology, bulk chemistry of the iron formation, and variations in prograde and retrograde metamorphism. The presence of amphiboles in the Ironwood is a known issue that will need to be factored into any future mine plans. This study provides an objective assessment of the distribution and character of amphiboles in the Ironwood to aid all decision-makers in any future resource development scenarios.

Introduction

Metamorphism of banded iron formations (BIFs) – the most important source of iron ore globally – commonly results in the formation of Fe-rich amphiboles in the ores at appropriate metamorphic grades. Amphiboles are found in metamorphosed BIFs throughout the world (Klein, 2005). Various terms have been used to describe the morphology of amphibole particles, such as massive, equant, prismatic, fibrous, and asbestiform. The definitions for these terms can be found below in the Methods section. The term “elongate mineral particle” (EMP) has been used by the regulatory community for a variety of mineral habits including prismatic, fibrous, and asbestiform particles, as well as cleavage fragments (NIOSH, 2011). Because of the links between *commercial asbestiform* amphibole minerals, mesothelioma, and lung cancer (Gibbs and Berry, 2008; Berry and Gibbs, 2008), concerns about potential human-health risks due to exposure non-asbestiform Fe amphiboles during mining and milling of metamorphosed BIF ores (taconite) have persisted. Interest in potential links between fibrous amphiboles and human health in the Lake Superior region began in earnest in the early 1970s related to airborne emissions around a taconite mill on the shore of Lake Superior and the since-banned practice of disposing of mill tailings at the bottom of the lake, which resulted in amphibole fibers appearing in nearby municipal drinking water supplies (Berndt and Brice, 2008). This incident has prompted over four and a half decades of scientific research exploring links between human health and amphibole particles through a variety of pathways related to the mining and milling of taconite ores. Allen et al. (2014) found increased risks for mortality from lung cancer, mesothelioma, and some cardiovascular disease among taconite miners, but could not exclude non-occupational behaviors, such as smoking, as a contributor. Brunner et al. (2008) found that most (14 out of 15 with adequate work histories) of the mesothelioma cases found in a case study of northern Minnesota iron miners had identifiable source exposures to commercial asbestos in jobs held both inside and outside of the iron mining industry. Other studies investigating the incidence of lung cancer in Minnesota taconite miners found that miners have shown no increased risk of mortality due to lung cancer (Berry and Gibbs, 2008; Allen et al., 2015a,b). Further, a study comparing the incidence of mesothelioma and lung disease in the western (hematite-rich, non-amphibole-bearing) and eastern (non-asbestiform, amphibole-bearing) Mesabi Iron Range in northern Minnesota did not find a higher incidence of disease in the amphibole-bearing portion of the mining district (Mandel and Odo, 2018). Only a few studies have investigated the role of asbestiform and non-asbestiform amphiboles in relation to lung cancer and mesothelioma. In laboratory studies, Mossman (2008) found that (non-asbestiform) cleavage fragments are less bioreactive and cytotoxic than asbestiform amphiboles. Gamble and Gibbs (2008), on the basis of a review of cohort studies, concluded that non-asbestiform amphiboles do not increase the risk of lung cancer or mesothelioma. In other words, for naturally occurring amphiboles encountered in taconite mining, a link between non-asbestiform cleavage fragments and disease has not been established, and a link between naturally occurring asbestiform amphibole and disease is unclear. Thus, the long history of controversy surrounding iron mining, amphibole minerals, and human health in northern Minnesota, and the apparent human-health significance of cleavage fragments of amphibole versus asbestiform amphiboles highlight the importance of an increased understanding of the nature and distribution of amphiboles in the nearby Gogebic Iron Range of northern Wisconsin from the perspective of informed decision-making related to future potential development of these resources.

The geological conditions that resulted in the formation of cummingtonite-grunerite in the Biwabik Iron Formation in Minnesota are analogous to those in the Ironwood Iron-Formation in Wisconsin. At both localities, the emplacement of a mafic intrusive body truncated the strata and caused contact metamorphism of the iron formation. Due to the similarity in geological conditions and the presence of cummingtonite-grunerite in the Ironwood Iron-Formation, many of the issues faced in Minnesota will be important when considering the possibility of mining in the Gogebic Iron Range.

Past studies have described the geology, petrography, and nature of metamorphism in the Ironwood (Laybourn, 1979; Cannon et al., 2007). The present study focuses on providing detailed mineralogical information about the origin, distribution, morphology, and chemistry of amphiboles in the Ironwood. In light of the historical issues associated with taconite mining in Minnesota and the complex problems posed by amphiboles with respect to human-health risk evaluation, the presence of amphiboles in the Ironwood warrants detailed characterization. The purpose of this study is to provide a mineralogical framework for the amphiboles that occur in the Ironwood to aid regulatory, medical, and mining entities in their evaluation of this potential resource. This study is based on a systematic sampling of the Ironwood from drill holes covering 35 km of strike length from its contact with the Mellen Intrusive Complex (MIC) in the west toward lower metamorphic grade in the east. Additionally, surface outcrops were sampled where available. Optical microscopy, X-ray diffraction, scanning electron microscopy, and electron microprobe analysis were used to characterize the amphiboles in the Ironwood Iron-Formation.

Setting

The Gogebic Iron Range historically has produced significant amounts of “natural” (supergene) iron ore but has yet to produce any “taconite” (ore that requires concentration of magnetite prior to smelting, otherwise known as “concentration-grade ore”), which is the focus of potential future development in the region. From 1877 to 1967, the Gogebic Iron Range produced approximately 325 million tons of “natural” ores (Cannon et al., 2007). These natural ores comprise nearly pure iron oxides and hydroxides that formed as secondary concentrations resulting from the structurally focused flow of deeply circulating, oxygenated groundwater that both oxidized the original iron minerals and replaced the chert with iron minerals (Cannon et al., 2007; Irving and Van Hise, 1892). The natural ores produced from the Gogebic are restricted to areas of very low-grade metamorphism, as even modest metamorphic recrystallization inhibited their formation (James, 1955; Cannon et al., 2007). Although concentration-grade ore has not been mined from the Gogebic, the western portion of the Ironwood constitutes one of the largest undeveloped iron resources in the United States. The study area, a 35-km east-west trending portion of the Ironwood (Figure 1), has been estimated to contain approximately 3.7 billion tons of taconite (Mardsen, 1978; Cannon et al., 2007).

The 1.87 Ga Ironwood Iron-Formation is a classic BIF in the Lake Superior Region that formed in a shallow sea resulting from extension and subsidence of the Superior craton associated with the approximately 1.88-1.84 Ga Penokean Orogeny (Cannon et al., 2007; Schulz and Cannon, 2007). The Ironwood was divided by Hotchkiss (1919) into five members: from the base upward, these are the Plymouth, Yale, Norrie, Pence, and Anvil Members. The Anvil Member is only found in the eastern portion of the range, outside of the study area. The Ironwood conformably overlies the Palms Formation, an argillite unit that transitions upwards to quartzite, which was deposited in a tidal environment and grades upward over several meters into the Ironwood, marking the transition from clastic to chemical sedimentation (Ojakangas, 1983; Cannon et al., 2007). The Ironwood is overlain by the Tyler Formation in the study area, a turbiditic unit primarily composed of black shale and greywacke. The Ironwood was intruded by diabase and gabbro dikes and sills of Paleoproterozoic and/or Mesoproterozoic age (Cannon et al., 2007). Several large gabbroic sills are concordant with the Ironwood, whereas numerous diabase dikes cut the Ironwood at high angles, forming both northeast- and northwest-trending sets. These mafic intrusions were commonly exposed in mine workings in the formerly active portions of the central Gogebic Iron Range, where they played an important role in controlling the location and distribution of natural iron ore bodies (Cannon et al., 2007).

In the western portion of the study area, the Ironwood is truncated by Mesoproterozoic gabbro of the Mellen Intrusive Complex. The Mellen Intrusive Complex was emplaced roughly parallel with the Ironwood and approximately coeval with northward tilting of the region during events related to the Midcontinent Rift at about 1.1 Ga; these units dip northward at approximately 70 degrees on average (Cannon et al., 1993; 1996; 2007). The primary effect of this intrusion was broad contact metamorphism, with metamorphic grade being most intense in the west, and diminishing eastward as the distance between the Ironwood and the Mellen Intrusive Complex increases (Cannon et al., 2007). Laybourn (1979) divided the Ironwood into four metamorphic zones. Zone 1 experienced diagenetic alteration/low-grade metamorphism and is defined by the presence of the Fe-phyllosilicates, minnesotaite and stilpnomelane, and Fe-bearing carbonates such as, siderite, dolomite, and ankerite. Zone 2 was characterized by medium-grade metamorphic conditions that resulted in the disappearance of Fe-phyllosilicates and Fe-bearing carbonates and the appearance of amphibole. Zone 3 underwent high-grade metamorphism and is defined by the presence of pyroxenes that developed from amphiboles. Zone 4 represents the highest grade of metamorphism where the development of fayalite is observed and occurs within 100 meters of the intrusive contact (Laybourn, 1979). Retrograde amphibole is also observed in Zones 3 and 4. These zones are similar to the progressive contact metamorphism documented in the Biwabik Iron-Formation in Minnesota due to the intrusion of the Duluth Complex (Gundersen and Schwartz, 1962; French, 1968).

Methods

Sample collection of the Ironwood Iron-Formation encompassed several outcrop locations and four diamond drill cores ranging from 0 to approximately 5 km from the contact with the Mellen Intrusive Complex (Figure 1). Each drill hole was collared in the Pence Member and ended in the upper quartzite unit of the Palms Formation, thus providing between 171 and 237 m of continuous core sampling. Drill hole MP-67-1 was directionally drilled at an unknown azimuth at angles varying from approximately 60° to 80°, drill hole W-156 was drilled at an azimuth of 180º and an angle of 40º, drill hole 666-1 was drilled at an azimuth of 180° and a 45° angle, and drill hole 186C was drilled at an azimuth of 156º and an angle of 45º. Two types of samples were selected from drill cores: a set from each lithologic sub-unit intended to be representative of the section, and a topical set that could potentially yield insights about the paragenesis of amphiboles. One hundred fifteen samples were collected and made into polished thin sections, which were examined using transmitted and reflected light microscopy. Areas of interest were then examined using a Hitachi SU5000 field emission scanning electron microscope equipped with an EDAX Octane Plus 30 mm^2 silicon drift detector for energy dispersive spectroscopy (SEM/EDS). EDS was used to confirm mineralogy. Using SEM imagery, amphibole morphology was characterized using a standardized grid designed to limit selective bias (Green, 2017) to provide morphological and geometric data.

Amphiboles from 17 representative samples were categorized according to morphological definitions adapted from Campbell et al. (1977) including: massive, equant, prismatic, and fibrous. Massive amphibole particles are tightly packed with scarcely distinguishable grain boundaries and are arranged in a homogenous structure. Equant particles are those with three approximately equally spaced dimensions, whereas prismatic particles are those with one elongate dimension and two approximately equal shorter dimensions. Fibrous particles are those with high aspect ratios, often displaying curvature and occurring in bundles. The minimum aspect ratio necessary to apply the term fibrous is generally 3:1 according to most regulatory bodies, such as the International Organization for Standardization and the National

Institute for Occupational Safety and Health (International Organization for Standardization, 1995; NIOSH, 2011), but this is often constrained by a maximum particle width of 3 μm (Lowers and Meeker, 2002). A drawback of observing amphibole particles in thin section is the inability to determine whether particles possess the properties of flexibility or high tensile strength. Both properties are inherent to the definition of asbestiform minerals, which are a subset of fibrous minerals that may not otherwise exhibit these features (Campbell et al., 1977). Having no means of demonstrating the properties of flexibility or high tensile strength, it is inappropriate to describe the amphiboles identified in this study as asbestiform based on the information currently available.

A total of 437 amphibole particles of prismatic, equant, and fibrous morphologies was measured using the software program QuartzPCI to determine geometric parameters. Massive particles were not measured because by definition, their boundaries were indistinct. Fibrous amphiboles were identified using ISO 10312 criteria for phase-contrast microscopy equivalent (PCME) fibers (length > 5 μm, width between 0.25 and 3 μm, and aspect ratio > 3:1) which are the basis for most health studies related to cancers in humans caused by asbestos exposure (International Organization for Standardization, 1995; U.S. Environmental Protection Agency, 2005).

A PANalytical X`Pert PRO diffractometer, X-ray diffraction (XRD) was used to determine the presence of amphiboles and modal mineral abundances, aided by Rietveld refinement using HighScore Plus v.4.5. A JEOL JXA-8900 electron microprobe analyzer utilizing wavelength-dispersive spectroscopy (EMPA-WDS) was employed to determine the chemistry of various minerals. Additional details concerning XRD and EMPA-WDS methods can be found by consulting Green et al. (2019).

This is a preprint, the final version is subject to change, of the American Mineralogist (MSA)
Cite as Authors (Year) Title. American Mineralogist, in press.
DOI: https://doi.org/10.2138/am-2020-7211

Results

Amphibole formation and distribution

The four metamorphic zones of the Ironwood are defined by their predominant mineral assemblages, which primarily changed with variations in temperature. Magnetite and chert are ubiquitous throughout the study area, whereas variations in the presence and species of Fe-silicates indicate changes in metamorphic conditions. Zone 1 is characterized by the presence of minnesotaite, stilpnomelane, dolomite, ankerite, and siderite. Maximum temperatures in Zone 1 reached approximately 300-340º C during diagenetic alteration/low-grade metamorphism, which is the upper stability limit of the Fe-phyllosilicates and Fe-carbonates characteristic of this zone (French, 1973; Frost et al., 2007). In Zone 2, which lies approximately 2.5 to 3.5 km from the Mellen Intrusive Complex, medium-grade metamorphism resulted in the dehydration and decarbonation of low-temperature minerals and the development of cummingtonite-grunerite and actinolite-ferro-actinolite by the following reactions (French, 1968; Bonnichsen, 1975; Frost, 1979 (observed in the Mesabi range); Laybourn, 1979 (observed in the Ironwood)):

1) $\underbrace{7Fe_3Si_4O_{10}(OH)_2}_{\text{minnesotaite}} = \underbrace{3Fe_7Si_8O_{22}(OH)_2}_{\text{grunerite}} + \underbrace{4SiO_2}_{\text{quartz}} + 4H_2O$ (Figure 2a)

2) $\underbrace{5Ca(Fe,Mg)(CO_3)_2}_{\text{ankerite}} + \underbrace{8SiO_2}_{\text{quartz}} + H_2O = \underbrace{Ca_2(Fe,Mg)_5Si_8O_{22}(OH)_2}_{\text{actinolite}} + \underbrace{3CaCO_3}_{\text{calcite}} + 7CO_2$

3) $\underbrace{7FeCO_3}_{\text{siderite}} + \underbrace{8SiO_2}_{\text{quartz}} + H_2O = \underbrace{Fe_7Si_8O_{22}(OH)_2}_{\text{grunerite}} + 7CO_2$ (Figure 2b)

Zone 3 occurs in the western portion of the study area where the Ironwood is less than approximately 2.5 km from the Mellen Complex up to within approximately 100 m from the contact between these units. High-grade metamorphism in this zone resulted in the development of pyroxenes from amphiboles by the following reactions (Bonnichsen, 1975 (observed in the Mesabi range); Laybourn, 1979 (observed in the Ironwood)):

4) $Ca_2(Fe,Mg)_5Si_8O_{22}(OH)_2 + 3CaCO_3 + 2SiO_2 = 5Ca(Fe,Mg)Si_2O_6 + 3CO_2 + H_2O$
actinolite calcite quartz hedenbergite

5) $Fe_7Si_8O_{22}(OH)_2 = 7FeSiO_3 + SiO_2 + H_2O$ (Figure 2f)
grunerite ferrosilite quartz

Retrograde metamorphism in this zone also resulted in the development of fine-grained grunerite as reaction 5 proceeded in the opposite direction (Bonnichsen, 1969). Textural evidence that this grunerite is retrograde includes the embayment of orthopyroxene by fine-grained grunerite (Figure 2d) and the occurrence of fine-grained grunerite aggregates that replace larger prismatic grunerite crystals (Figure 2e).

Zone 4 occurs in the far western portion of the study area within 100 m of the contact between the Ironwood and the Mellen Complex. Maximum temperatures of approximately 700º C resulted in the development of fayalite by the following reaction, which is unique to this small, restricted zone (French, 1968 (observed in the Mesabi Range); Laybourn, 1979 (observed in the Ironwood)):

6) $2Fe_7Si_8O_{22}(OH)_2 = 7Fe_2SiO_4 + 9SiO_2 + 2H_2O$
grunerite fayalite quartz

Retrograde amphibole is observed intergrown with pyroxene and fayalite. Having been consumed during reaction 6, prograde amphibole is not observed in these samples, although it has been reported in Zone 4 by Laybourn (1979).

The extent and location of each of these zones was determined by the mineralogical associations observed by optical microscopy and XRD analysis of drill core and outcrop samples throughout the study area. In Zones 2, 3, and 4, amphiboles are present in abundance in each member of the Ironwood. The prevalence of low-grade mineral assemblages in Zone 1 indicates that the Ironwood in Zone 1 generally did not reach temperatures high enough to produce amphibole. Observation of drill core samples in Zone 1 (drill holes 666-1 and 186C), however, revealed the localized presence of amphiboles among a predominantly low-grade mineral assemblage comprising Fe-carbonates and Fe-phyllosilicates (Figure 3). Within drill hole 666-1, the presence of amphibole in minor to trace quantities was observed solely at a depth of approximately 240-270 m. Within this range, the presence of two diabase dikes are noted in the core logs. Within drill hole 186C, the presence of amphibole in major quantities was observed solely at depths of 10 to 40 m; however, no dikes were observed within or near those samples.

Morphology and geometry

The various habits of amphibole in the Ironwood are commonly intergrown or found in proximity to one another (Figure 4). In order to provide a representation of the frequency with which various amphibole habits occur in the Ironwood, amphibole-bearing areas were characterized using a systematic method of observation. Within the areas that were observed in thin section from a set of samples in which amphibole is a major constituent, 63% and 25% of the areas contained massive and prismatic amphiboles, respectively. These are the most common habits assumed by amphiboles in the Ironwood. Less common forms include equant and fibrous morphologies, which were each observed in 6% of the areas examined. Fibrous amphiboles, which have potential human-health and environmental impacts, were identified in each of the drill holes sampled in this study, but were not observed in outcrop samples. Fibrous amphiboles were observed in the Pence, Norrie, and Plymouth Members of the Ironwood, which comprise the potential ore zones; whereas, no fibrous amphiboles were observed in the Yale Member, which is considered to be waste rock due to its high silica and low magnetite content (Figure 3).

Cumulative frequency distributions of length, width, and aspect ratios for 437 amphibole particles are displayed in Figure 5. A difficulty inherent to classifying the morphology and geometry of amphiboles in thin section is the random orientation of mineral particles, which may obscure their maximum dimensions. Therefore, measurements of amphibole particles presented in Figure 5 are potentially minimum values, and represent only prismatic, fibrous, or equant particles. Massive particles were not measured because, by definition, they are homogenous with indistinct grain boundaries.

Amphibole chemistry

The amphiboles that occur in the Ironwood are members of the monoclinic Mg-Fe-Mn-amphibole group and the Ca-amphibole group (Hawthorne et al., 2012). These amphiboles are chemically simple and consistent with published values of amphiboles from BIF occurrences globally (Table 1). The most common species observed include members of the cummingtonite-grunerite series (Figure 6) and the actinolite-ferroactinolite series; whereas members of the magnesio-hornblende-ferro-hornblende series are relatively uncommon (Figure 7). Members of these two groups are frequently intergrown. Mg-Fe-Mn-group amphiboles occur with greater frequency than do Ca-group amphiboles, the formation of which is dependent upon the presence of dolomite-ankerite and/or stilpnomelane in the protolith. Among amphiboles of all groups, variations in their chemistry are observed primarily as changes in the Mg#, ranging from highly ferrous to highly magnesian. Factors that may influence the Mg# include the presence of coexisting minerals that can incorporate or buffer Fe and Mg, bulk chemistry of the iron-formation, temperature of amphibole formation, amphibole morphology, and variations in prograde and retrograde metamorphic reactions.

The range of molar Mg/(Mg+Fe^{2+}) values (Mg#) is similar in massive and prismatic amphiboles and spans from 0.06 to 0.87, representing both the most Fe- and Mg-rich compositions. In contrast, the Mg# of fibrous amphiboles, regardless of their location, is restricted to values of 0.14 to 0.35 (Figure 8). Analyses of fibrous grunerite reveal that among these restricted values, Mg# increases concomitant with true distance (the actual distance between the units as opposed to the geographic distance observed at the surface) from the Mellen Intrusive Complex (Figure 9). The relationship between the amphibole Mg# and distance from the Mellen Intrusive Complex has implications for the peak temperature of metamorphism, variations in which may result in changes in Mg# values. Because the dips of the Ironwood and the Mellen Intrusive Complex are roughly parallel, an increase in drill-hole depth results in increasing distance from the intrusive body accompanied by a decrease in temperature. However, the magnitude of heat flux within a drill hole as a function of depth is not likely to produce significant compositional variation in amphiboles. Rather, compositional variation with depth appears to be a function of bulk composition of the Ironwood. Variations in the range of Mg# values in amphiboles between various zones may in part be a function of the predominant mineral assemblage. As amphibole is the primary mineral capable of incorporating Mg in drill hole W-156 (Zone 2), the wide degree of compositional variation observed in this drill hole may be explained by the general lack of coexisting minerals capable of accommodating Mg. In contrast, outcrop samples (Zone 4) and drill hole MP-67-1 (Zone 3) contain abundant pyroxene, whereas drill holes 666-1, and 186C (Zone 1) contain abundant dolomite. EMPA data indicate that these minerals incorporate significant Mg, which may result in relatively Fe-rich amphiboles (see Green et al., 2019 for EMPA results).

Prograde and retrograde grunerite, distinguished previously on the basis of textural evidence, can also be identified by chemical composition. Analyses show that prograde grunerites are relatively enriched in Mn but fall within the range of Mg# values exhibited by retrograde grunerite (Figure 10).

Discussion

Amphibole spatial distribution

The development of amphibole in the Ironwood was previously considered to be solely resulting from pervasive contact metamorphism related to the emplacement of the Mellen Intrusive Complex. This conclusion was based upon samples from exposed outcrops, which, while abundant in the western and central portions of the study area, are lacking in the eastern portion (Laybourn, 1979). Based upon variations in pervasive mineral assemblages, the zone of amphibole development and the conditions permitting it are theoretically restricted to Zones 2-4, where temperatures exceeded 300-340º C. Access to drill-core samples in Zone 1, however, revealed the localized presence of amphibole at depth (Figure 3), in contrast to previous conclusions about the extent of amphibole development. The mineralogical character of drill holes 666-1 and 186C is that of a low-grade metamorphic assemblage primarily comprising dolomite, ankerite, magnetite, chlorite, and chert, indicating that the bulk of this portion of the Ironwood was not subjected to temperatures in excess of 300-340º C. The presence of grunerite isolated at 240-270 m depth within drill hole 666-1 is likely dependent upon localized metamorphism of the Ironwood that did not generate a pervasive heat flux. If the heat generated by the emplacement of the Mellen Intrusive Complex was responsible for grunerite development at 240-270 m depth in this location, the shallower portions of the drill core, which are closer to the contact with the Mellen Complex, would have necessarily been subjected to even greater temperatures, which would have altered the low-grade assemblage and produced pervasive amphibole-bearing assemblages. The absence of pervasive amphibole development as observed in Zones 2-4 and the localized development of grunerite at depth in Zone 1 suggest an alternate mechanism of localized metamorphism, such as the emplacement of mafic dikes and/or sills. In fact, diabase dikes that cut the Ironwood at nearly right angles to bedding were commonly identified in underground mine workings in the formerly active part of the central Gogebic Iron Range. Although seldom seen in natural exposures, the presence of diabase dikes is indicated in drill core logs from the study area and directly observed in drill core samples (Figure 2c). Based on this evidence, the presence of amphibole in the Ironwood Iron-Formation cannot be constrained solely to Zones 2 to 4 but may also result from localized contact metamorphism by diabase dikes in Zone 1. Previous work indicates that changes in CO_2 content have minimal effect on expanding the stability field of amphibole; therefore, the development of amphibole in Zone 1 is likely dependent on localized temperature increases caused by mafic intrusions (Frost, 1979).

Whereas the presence of fibrous amphiboles in the Ironwood has not been unambiguously linked to a particular set of structural features or hydrothermal processes, various conditions imperative to their formation exist within the study area. High-strain environments within folds, shear planes, faults, dilation cavities, and at intrusion-host rock boundaries potentially permit the primary crystallization of fibrous amphiboles from hydrothermal solutions

(Ross et al., 2008). Fibrous amphiboles may also form as low-temperature alteration products of non-fibrous amphiboles (Ross et al., 2008). Thrust faults and folds of various scales that formed during the Penokean orogeny and Mesoproterozoic northward tilting are widespread throughout the study area, particularly near Mount Whittlesey where intense deformation resulted in highly complex structures (Cannon et al., 1993; 2007).

Implications

Previous studies of the Ironwood established the zoned nature of contact metamorphism which was thought to accurately constrain the extent of amphibole development in the Ironwood. Results of extensive sampling conducted during this study are in close accord with the original location of these zones. However, this study presents evidence of amphiboles in the Ironwood independent of the influence of the contact metamorphic aureole resulting from the emplacement of the Mellen Intrusive Complex and extends the potential amphibole-bearing areas as far east as the town of Upson. The identification of localized amphibole development in zones of low-grade metamorphic conditions suggests localized metamorphism resulting from the intrusion of diabase dikes approximately normal to bedding in the Ironwood.

A salient global issue related to the mining of metamorphosed banded iron formations is the presence of amphibole minerals and their morphology because of human-health concerns related to elongate mineral particles. The human-health risks center on particle size and aspect ratio. The taconite production process generates large volumes of siliceous tailings, which are typically divided into coarse and fine fractions. The coarse fraction consists of material generally less than 10 mm in size, and contains less than 10% fine material, which is defined as material that passes through a 200-mesh sieve (approximately 75 µm or less). Processes in which amphibole particles may be released to the environment include drilling and blasting at the mine site, loading and hauling to the processing plant, comminution, and tailings disposal. Some taconite operations allow the coarse and fine fractions to flow together as a slurry to the same location, rather than separating them (Zanko et al., 2008). Nearly one hundred per cent of amphibole EMP measured in this study display lengths and widths less than 75 µm (Figure 5a, 5b). This indicates that the comminution (grinding) and separation stages of ore processing would segregate amphibole EMP in the Ironwood into the fine tailings fraction. Therefore, in areas where amphibole EMP exist these fine-grained particles that have the potential to be classified as fibers under regulatory definitions may be produced during taconite processing and reside in the tailings storage facility.

The presence of amphibole within each drill hole examined in this study, and in the potential ore and waste rock zones of the Ironwood necessitates a comprehensive plan for solid waste management if a mine is ever put into operation. The comminution process will break down all types of amphibole particles resulting in the production of fine-grained EMP. However, it is noteworthy that non-asbestiform amphiboles do not appear to increase risk of lung cancer or mesothelioma (Gamble and Gibbs, 2008).

In the absence of a proposed mine plan, it is only possible to speculate about ore processing and waste management strategies, both of which will influence potential human-health risks. The experience in Minnesota with amphibole-bearing taconite tailings will allow for better informed decisions to be made about the potential future mine development in Wisconsin. The historical appearance of amphibole particles in drinking water supplies derived from Lake Superior indicates that disposal of tailings in Lake Superior is untenable (Berndt and Brice, 2008). For land-based disposal, erosion of tailings piles and windblown dusts are the main concerns. Erosion control and dust suppression are common challenges at mines, with which the mining industry has considerable experience (Mills and Clar, 1976; Evans, 2000; Reed et al., 2008).

As a large undeveloped iron resource capable of solely providing several decades of domestic supply (U.S. Geological Survey, 2018), the Ironwood will continue to garner interest. Potential development of this resource must be predicated on a thorough understanding of the amphiboles in the Ironwood and detailed strategies to mitigate environmental and human-health risks associated with them. Understanding how various factors contribute to the human-health risk of exposure to fibrous amphibole particles is a complex challenge that draws upon a variety of disciplines. The data presented in this study provide a framework upon which further mineralogical, medical, and biological work can expand to better understand the potential impacts of developing iron resources affected by metamorphism throughout the world.

ACKNOWLEDGEMENTS

This work was conducted under a Technical Assistance Agreement between the USGS and Congdon Minerals Management, Inc. This company permitted access, description, and sampling of the four proprietary drill cores and outcrops described here. The authors wish to acknowledge David Meineke, Paul Eger, and Stacy Saari of Global Minerals Engineering, and David Adams of Congdon Minerals Management, Inc. for their logistical and technical assistance as well as Robert Hazen for review and support. Any use of trade, firm, or product names is for descriptive purposes only and does not imply endorsement by the U.S. Government.

REFERENCES

Allen, E.M., Alexander, B.H., MacLehose, R.F., Ramachandran, G., and Mandel, J.H., 2014. Mortality experience among Minnesota taconite mining industry workers. Occupational and Environmental Medicine, vol. 71, p. 744-749, https://doi.org/10.1136/oemed-2013-102000.

Allen, E.M., Alexander, B.H., MacLehose, R.F., Nelson, H.H., Ramachandran, G., and Mandel, J.H., 2015a. Cancer incidence among Minnesota taconite mining industry workers. Annals of Epidemiology, vol. 25, p. 811-815, https://doi.org/10.1016/j.annepidem.2015.08.003.

Allen, E.M., Alexander, B.H., MacLehose, R.F., Nelson, H.H., Ryan, A.D., Ramachandran, G., and Mandel, J.H., 2015b. Occupational exposures and lung cancer risk among Minnesota taconite mining workers. Occupational and Environmental Medicine, vol. 72, p. 633-639, https://doi.org/10.1136/oemed-2015-102825.

Berndt, M.E., and Brice, W.C., 2008. The origins of public concern with taconite and human health: Reserve Mining and the asbestos case. Regulatory Toxicology and Pharmacology, vol. 52, S31-S39.

Berry, G., and Gibbs, G.W., 2008. An overview of the risk of lung cancer in relation to exposure to asbestos and of taconite miners. Regulatory Toxicology and Pharmacology, vol. 52, S218-S222.

Bonnichsen, B., 1969. Metamorphic pyroxenes and amphiboles in the Biwabik Iron-Formation, Dunka River Area, Minnesota. Mineralogical Society of America Special Papers, vol. 2, p. 217-239.

Bonnichsen, B., 1975. Geology of the Biwabik Formation, Dunka River Area, Minnesota. Economic Geology, vol. 70, p. 319-340.

Brunner, W.M., Williams, A.N., and Bender, A.P., 2008. Investigation of exposures to commercial asbestos in northeastern Minnesota iron miners who developed mesothelioma. Regulatory Toxicology and Pharmacology, vol. 52, S116-S120.

Campbell, W.J., Blake, R.L., Brown, L.L., Cather, E.E., and Sjoberj, J.J., 1977. Selected silicate minerals and their asbestiform varieties: Mineralogical definitions and identification-characterization. U.S. Bureau of Mines, Information Circular 8751, 55 p.

Cannon, W.F., Peterman, Z.E., and Sims, P.K., 1993. Crustal-scale thrusting and origin of the Montreal River Monocline, a 35-km-thick cross section of the Midcontinent Rift in northern Wisconsin and Michigan. Tectonics, v. 12, no. 3, p. 728–744.

Cannon, W.F., Woodruff, L.G., Nicholson, S.W., and Hedgman, C.A., 1996. Bedrock geologic map of the Ashland and the northern part of the Ironwood 30’ x 60’ quadrangles, Wisconsin, and Michigan. U.S. Geological Survey, Miscellaneous Geologic Investigations Map I-2566.

Cannon, W.F., LaBerge, G.L., Klasner, J.S., and Schulz, K.J., 2007. The Gogebic iron range—A sample of the northern margin of the Penokean fold and thrust belt. U.S. Geological Survey Professional Paper 1730, 44 p.

Evans, K., 2000. Methods for assessing mine site rehabilitation design for erosion impact. Australian Journal of Soil Research, vol. 38, p. 231-248.

French, B.M., 1968. Progressive contact metamorphism of the Biwabik Iron-Formation, Mesabi Range, Minnesota. Minnesota Geological Survey Bulletin, 45, 103 p.

French, B.M., 1973. Mineral assemblages in diagenetic and low-grade metamorphic iron-formation. Economic Geology, vol. 68, p. 1063-1075.

Frost, B.R., 1979. Metamorphism of Iron-Formation: Parageneses in the system Fe-Si-C-O-H. Economic Geology, vol. 74, p. 775-785.

Frost, C.D., von Blanckenburg, F., Schoenberg, R., Frost, B.R., and Swapp, S.M., 2007. Preservation of Fe isotope heterogeneities during diagenesis and metamorphism of banded iron formation. Contributions to Mineralogy and Petrology, vol. 153, p. 211-235.

Gamble, J.F., and Gibbs, G.W., 2008. An evaluation of the risks of lung cancer and mesothelioma from exposure to amphibole cleavage fragments. Regulatory Toxicology and Pharmacology, vol. 52, S154-S186.

Gibbs, G.W., and Berry, G., 2008. Mesothelioma and asbestos. Regulatory Toxicology and Pharmacology, vol. 52, S223-S231.

Green, C.J., 2017. Origin, distribution, morphology, and chemistry of amphiboles in the Ironwood Iron-Formation, Gogebic Iron Range, Wisconsin, USA. [MSc thesis]: Fairfax, VA, George Mason University, 42 p.

Green, C.J., Seal II, R.R., Cannon, W.F., Piatak, N.M., and McAleer, R.J., 2019. Chemistry, morphology, modal mineralogy, and photomicrographs of amphiboles and other minerals in the Ironwood Iron-Formation, Gogebic Iron Range, Wisconsin, USA (ver. 2.0, April 2019). U.S. Geological Survey data release, https://doi.org/10.5066/F7P84B41.

Gundersen, J.N., and Schwartz, G.M., 1962. The geology of the metamorphosed Biwabik iron-formation, Eastern Mesabi district, Minnesota. Minnesota Geological Survey Bulletin, 43, 139 p.

Hawthorne, F.C., Oberti, R., Harlow, G.E., Maresch, W.V., Martin, R.F., Schumacher, J.C., and Welch, M.D., 2012. IMA report, nomenclature of the amphibole supergroup. American Mineralogist, vol. 97, p. 2031–2048.

Hotchkiss, W.O., 1919. Geology of the Gogebic range and its relation to recent mining developments. Engineering and Mining Journal, v. 108, p. 443–452, 501–507, 537–541, and 577–582.

International Organization for Standardization, 1995. ISO 10312:1995, Ambient Air – Determination of Asbestos Fibres – Direct-Transfer Transmission Electron Microscopy Method. https://www.iso.org/standard/18358.html

Irving, R.D., and Van Hise, C.R., 1892. The Penokee iron-bearing series of Michigan and Wisconsin. U.S. Geological Survey Monograph 19, 534 p.

James, H.L., 1955. Zones of regional metamorphism in the Precambrian of northern Michigan. Geological Society of America Bulletin, vol. 66, p. 1455-1488.

Katsuta, N., Shimizu, I., Helmstaedt, H., Takano, M., Kawakami, S., Kumazawa, M., and Brown, M., 2012. Major element distribution in Archean banded iron formation (BIF): Influence of metamorphic differentiation. Journal of Metamorphic Geology, vol. 30, p. 457-472.

Klein, C., 2005. Some Precambrian banded iron-formations (BIFs) from around the world: Their age, geologic setting, mineralogy, metamorphism, geochemistry, and origin. American Mineralogist, vol. 90, p. 1473-1499.

Lafuente, B., Downs, R.T., Yang, H., and Stone, N., 2015. The power of databases: The RRUFF project. In: Highlights in Mineralogical Crystallography, T. Armbruster and R.M. Danisi, eds. Berlin, Germany, W. De Gruyter, p. 1-30.

Laybourn, D.P., 1979. The geology and metamorphism of the Ironwood Iron-Formation, Gogebic Range, Wisconsin. [MSc thesis]: Minneapolis, MN, University of Minnesota, 223 p.

Leake, B.E.,Woolley, A.R., Arps, C.E.S., Birch, W.D., Gilbert, M.C., Grice, J.D., Hawthorne, F.C., Kato, A., Kisch, H.J., Krivovichev, V.G., Linthout, K., Laird, J., Mandarino, J.A., Maresch, W.V., Nickel, E.H., Rock, N.M.S., Schumacher, J.C., Smith, D.C., Stephenson, N.C.N., Ungaretti, L., Whittaker, E.J.W., and Guo, Y., 1997. Nomenclature of amphiboles: Report of the subcommittee on amphiboles of the International Mineralogical Association, Commission on New Minerals and Mineral Names. Canadian Mineralogist, vol. 35, p. 219–246.

Lowers, H., and Meeker, G., 2002. Tabulation of asbestos-related terminology. USGS Open-File Rep. 02-458. USGS, Reston, VA. http://pubs.usgs.gov/of/2002/ofr-02-458/index.html.

Mandel, J.H., and Odo, N.U., 2018. Mesothelioma and other lung disease in taconite miners; the uncertain role of non-asbestiform EMP. Toxicology and Applied Pharmacology, vol. 361, p. 107-112.

Mardsen, R.W., 1978. Iron ore reserves of Wisconsin—A minerals availability system report. In Proceedings, American Institute of Mining Engineers, 51st annual meeting, Minnesota Section, Duluth, Minn., Jan. 11–13, 1978. University of Minnesota, American Institute of Mining Engineers, no. 39, p. 24-1 to 24-28.

Mills, T.R., and Clar, M.L., 1976. Erosion and sediment control; surface mining in the Eastern U.S.; planning and design. Hittman Associates, Columbia, Maryland. Prepared for U.S. Environmental Protection Agency, EPA-625/3-76-006, 238 p.

Mossman, B.T., 2008. Assessment of the pathogenic potential of asbestiform vs. nonasbestiform particulates (cleavage fragments) in *in vitro* (cell and organ culture) models and bioassays. Regulatory Toxicology and Pharmacology, vol. 52, S200-S203.

Mücke, A., and Annor, A., 1993. Examples and genetic significance of the formation of iron oxides in the Nigerian banded iron-formations. Mineralium Deposita, vol. 28, p. 136-145.

NIOSH, 2011. Asbestos Fibers and Other Elongate Mineral Particles: State of the Science and Roadmap for Research. Department of Health and Human Services, Centers for Disease Control and Prevention, National Institute for Occupational Safety and Health, 147 p.

Ojakangas, R.W., 1983. Tidal deposits in the early Proterozoic basin of the Lake Superior region; the Palms and the Pokegama Formations; evidence of subtidal-deposition of the superior-type banded iron-formation. In Medaris, L.G., Jr., ed., Early Proterozoic geology of the Great Lakes region. Geological Society of America Memoir 160, p. 49–56.

Reed, W., Listak, J.M., Page, S.J., and Organiscak, J.A., 2008. Summary of NIOSH research completed on dust control methods for surface and underground drilling. Society for Mining, Metallurgy, and Exploration, vol. 324, p. 32-40.

Ross, M., Nolan, R.P., and Nord, G.L., 2008. The search for asbestos within the Peter Mitchell Taconite iron ore mine, near Babbitt, Minnesota. Regulatory Toxicology and Pharmacology, vol. 52, p. S43-S50.

Schulz, K.J., and Cannon, W.F., 2007. The Penokean orogeny in the Lake Superior region. Precambrian Research, vol. 157, p. 4-25.

U.S. Environmental Protection Agency, 2005. U.S. EPA Asbestos Assessment for El Dorado Hills. San Francisco, California, https://archive.epa.gov/region9/toxic/web/pdf/eldorado-asb-flyer.pdf, 7 p.

U.S. Geological Survey, 2018. Mineral commodity summaries 2018. U.S. Geological Survey, 200 p., https://doi.org/10.3133/70194932.

Zanko, L.M., Niles, H.N., and Oreskovich, J.A., 2008. Mineralogical and microscopic evaluation of coarse taconite tailings from Minnesota taconite operations. Regulatory Toxicology and Pharmacology, vol. 52, p. S51–S65.

This is a preprint, the final version is subject to change, of the American Mineralogist (MSA)
Cite as Authors (Year) Title. American Mineralogist, in press.
DOI: https://doi.org/10.2138/am-2020-7211

List of figure captions:

FIGURE 1. Geologic map of the study area and sampling locations within the Ironwood Iron-Formation, after Cannon et al. (1996).

FIGURE 2. Transmitted light photomicrographs in plane-polarized (a, c) and cross-polarized (b, d, e, f) light of samples from the Ironwood Iron-Formation. **(a)** Mass of grunerite surrounded by sheaves of minnesotaite (sample 186C-64.0, Zone 1). **(b)** Grunerite developing from siderite (sample 666-1-813.5, Zone 1). **(c)** Diabase dike (left) cross-cutting relict iron oxide granules in a quartz matrix at a high angle relative to horizontal bedding (sample 666-1-485.0, Zone 1). **(d)** Development of retrograde grunerite from orthopyroxene (sample MP-67-1-205.0, Zone 3). **(e)** Replacement of prograde prismatic grunerite by fine-grained retrograde grunerite (sample MP-67-1-143.3, Zone 3). **(f)** Ferrosilite and grunerite (sample MP-67-1-532.5, Zone 3).

FIGURE 3. Stratigraphic representation of sampling locations and amphibole occurrences in the Ironwood Iron-Formation.

FIGURE 4. SEM micrographs showing examples of various amphibole morphologies in the Ironwood Iron-Formation. **(a)** Massive intergrowth of ferro- and magnesio-hornblende with magnetite (sample MP-67-1-607.5). **(b)** Interpenetrant prismatic grunerite crystals and an elongate grunerite crystal (length = 37 μm, width = 1.9 μm, sample MP-67-1-395.5). **(c)** Sprays of fibrous grunerite crystals (sample W-156-512.5). **(d)** Equant grunerite crystals and an elongate grunerite crystal (length = 67 μm, width = 4.7 μm, sample MP-67-1-395.5).

FIGURE 5. Cumulative frequency distribution of **(a)** lengths **(b)** widths, and **(c)** aspect ratios for amphibole particles in the Ironwood Iron-Formation.

FIGURE 6. The lower, iron-rich portion of the Mg-Mn-Fe ternary showing the compositions of monoclinic Mg-Fe-Mn-group amphiboles from various drill cores and outcrops of the Ironwood Iron-Formation (after Hawthorne et al., 2012).

FIGURE 7. Classification of the Ca-group amphiboles in the Ironwood Iron-Formation (after Leake et al., 1997). No Ca-group amphiboles were identified in drill hole 666-1.

FIGURE 8. $Mg/(Mg+Fe^{2+})$ values of all analyzed amphiboles in the Ironwood Iron-Formation separated by morphology.

FIGURE 9. Variation of Mg# with true distance from the Mellen Intrusive Complex of fibrous grunerites from the Ironwood Iron-Formation. Note: True distance accounts for the dip of both the Ironwood Iron-Formation and Mellen Intrusive Complex.

FIGURE 10. The lower, iron-rich portion of the Mg-Mn-Fe ternary showing the compositional variation between prograde and retrograde grunerite from drill hole MP-67-1 in the Ironwood Iron-Formation (after Hawthorne et al., 2012).

TABLE 1. Amphibole EMPA data from the Ironwood Iron-Formation compared to other BIF-hosted amphiboles. Refer to Green et al., 2019 for individual analyses.

Analysis (wt %)	Ironwood Iron-Formation Wisconsin, USA		Kushaka belt BIF Nigeria		Penge Mine South Africa		Bell Lake BIF Slave craton, Canada		
	Grunerite Avg (n=253)	Ferro-actinolite Avg (n=55)		Grunerite Avg (n=2)		Grunerite Avg (n=10)		Grunerite Avg (n=14)	Actinolite Avg (n=11)
SiO_2	49.37	50.65	SiO_2	49.06	SiO_2	50.51	SiO_2	51.70	53.22
TiO_2	0.03	0.04	TiO_2	-	TiO_2	0.02	TiO_2	0.00	0.01
Al_2O_3	0.73	0.66	Al_2O_3	0.19	Al_2O_3	0.20	Al_2O_3	0.23	0.54
Cr_2O_3	0.02	0.02	Cr_2O_3	-	Cr_2O_3	0.02	Cr_2O_3	0.00	0.00
MnO	1.35	0.95	MnO	2.51	MnO	0.63	MnO	0.73	0.30
FeO	36.73	28.07	FeO	40.68	FeO	38.78	FeO	35.83	23.04
Fe_2O_3	1.14	1.35	Fe_2O_3	0.46	Fe_2O_3	-	Fe_2O_3	-	-
MgO	6.22	5.48	MgO	4.69	MgO	6.65	MgO	8.72	9.45
CaO	1.09	10.79	CaO	0.37	CaO	0.12	CaO	0.73	11.70
Na_2O	0.12	0.13	Na_2O	-	Na_2O	0.07	Na_2O	0.03	0.07
K_2O	0.11	0.06	K_2O	-	K_2O	0.04	K_2O	0.00	0.00
F	0.00	0.00	F	-	F	0.04	F	-	-
Cl	0.12	0.11	Cl	-	Cl	0.02	Cl	-	-
H_2O	1.88	1.91	H_2O	1.86	H_2O	2.91	H_2O	-	-
Total	98.76	100.10	Total	99.80	Total	97.09	Total	97.98	98.34
Formula assignments									
based on - 24 (OH, F, Cl, O)			*24 (OH, F, Cl, O)*		*23 O*		*23 O*		
Si	7.90	7.86	Si	7.91	Si	8.03	Si	8.05	7.95
Al	0.21	0.17	Al	0.04	Fe^{2+}	5.16	Ti	0.00	0.00
Ti	0.01	0.01	Fe^{3+}	0.06	Mg	1.58	Al	0.04	0.10
Fe^{3+}	0.30	0.21	Fe^{2+}	5.51	Mn	0.08	Cr	0.00	0.00
Cr	0.00	0.00	Mg	1.10	Al	0.04	Fe^{3+}	0.00	0.17
Mn	0.18	0.21	Mn	0.34	Ca	0.02	Fe^{2+}	4.67	2.71
Fe^{2+}	4.92	3.68	Ca	0.06	Na	0.02	Mn	0.10	0.04
Mg	1.47	1.26	O	22.00	Sum T,C,B,A	14.92	Ni	0.00	0.00
Ca	0.19	1.79	OH	2.00			Mg	2.02	2.10
Na	0.04	0.04	Sum T,C,B,A	15.02			Ca	0.12	1.87
K	0.02	0.01					Na	0.01	0.02
O	22.00	22.00					K	0.00	0.00
OH	1.98	1.98					Sum T,C,B,A	15.01	14.96
F	0.00	0.00							
Cl	0.03	0.03							
Sum T,C,B,A	14.99	15.02							
			Mücke and Annor, 1993		Lafuente et al., 2015		Katsuta et al., 2012		

Figure 1

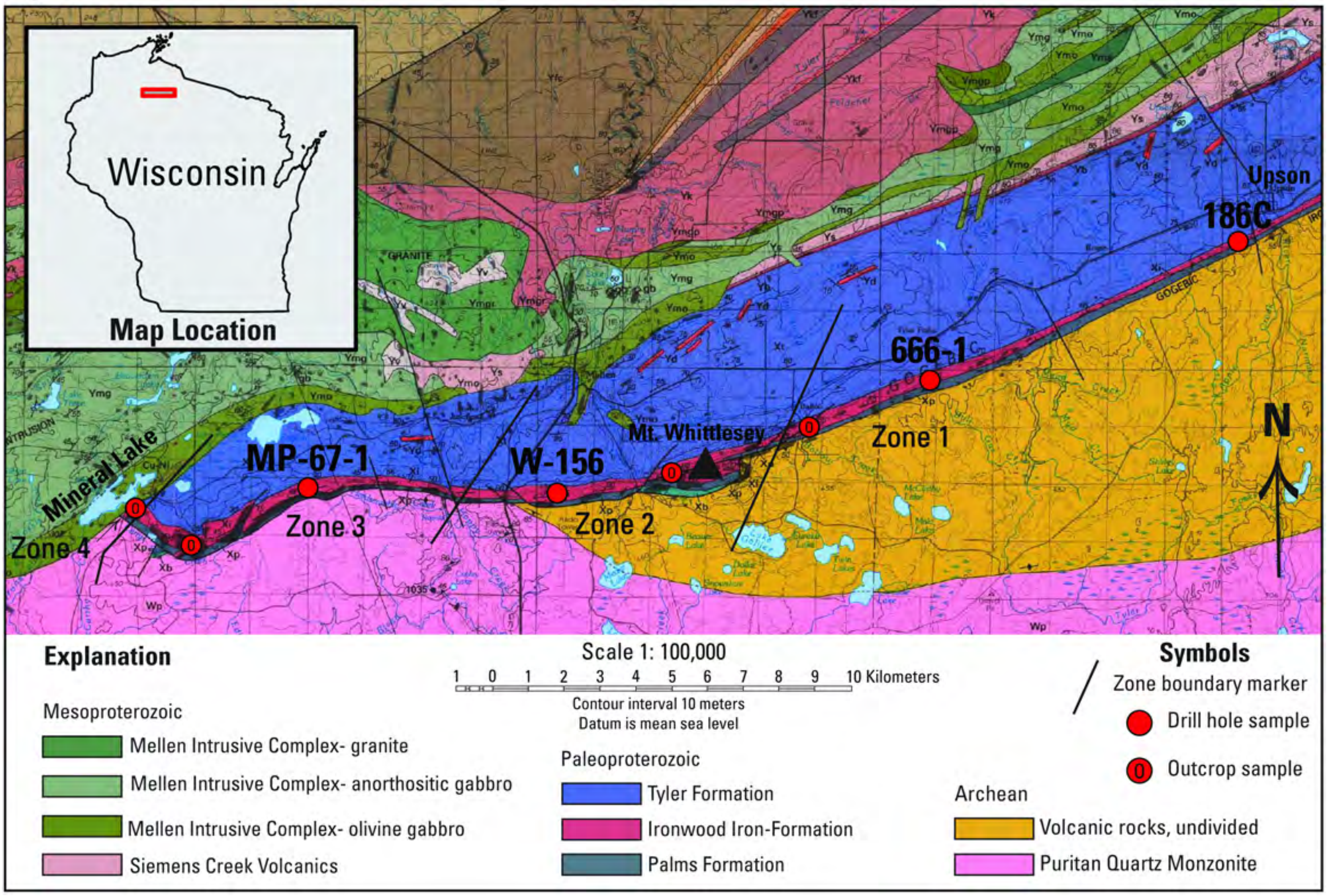
Wisconsin
Map Location
Mineral Lake
Zone 4
MP-67-1
Zone 3
W-156
Zone 2
Mt. Whittlesey
666-1
Zone 1
186C
Upson
N
Explanation
Mesoproterozoic
Mellen Intrusive Complex- granite
Mellen Intrusive Complex- anorthositic gabbro
Mellen Intrusive Complex- olivine gabbro
Siemens Creek Volcanics
Scale 1: 100,000
1 0 1 2 3 4 5 6 7 8 9 10 Kilometers
Contour interval 10 meters
Datum is mean sea level
Paleoproterozoic
Tyler Formation
Ironwood Iron-Formation
Palms Formation
Archean
Volcanic rocks, undivided
Puritan Quartz Monzonite
Symbols
Zone boundary marker
Drill hole sample
Outcrop sample

This is a preprint, the final version is subject to change, of the American Mineralogist (MSA)
Cite as Authors (Year) Title. American Mineralogist, in press.
DOI: https://doi.org/10.2138/am-2020-7211

Figure 2

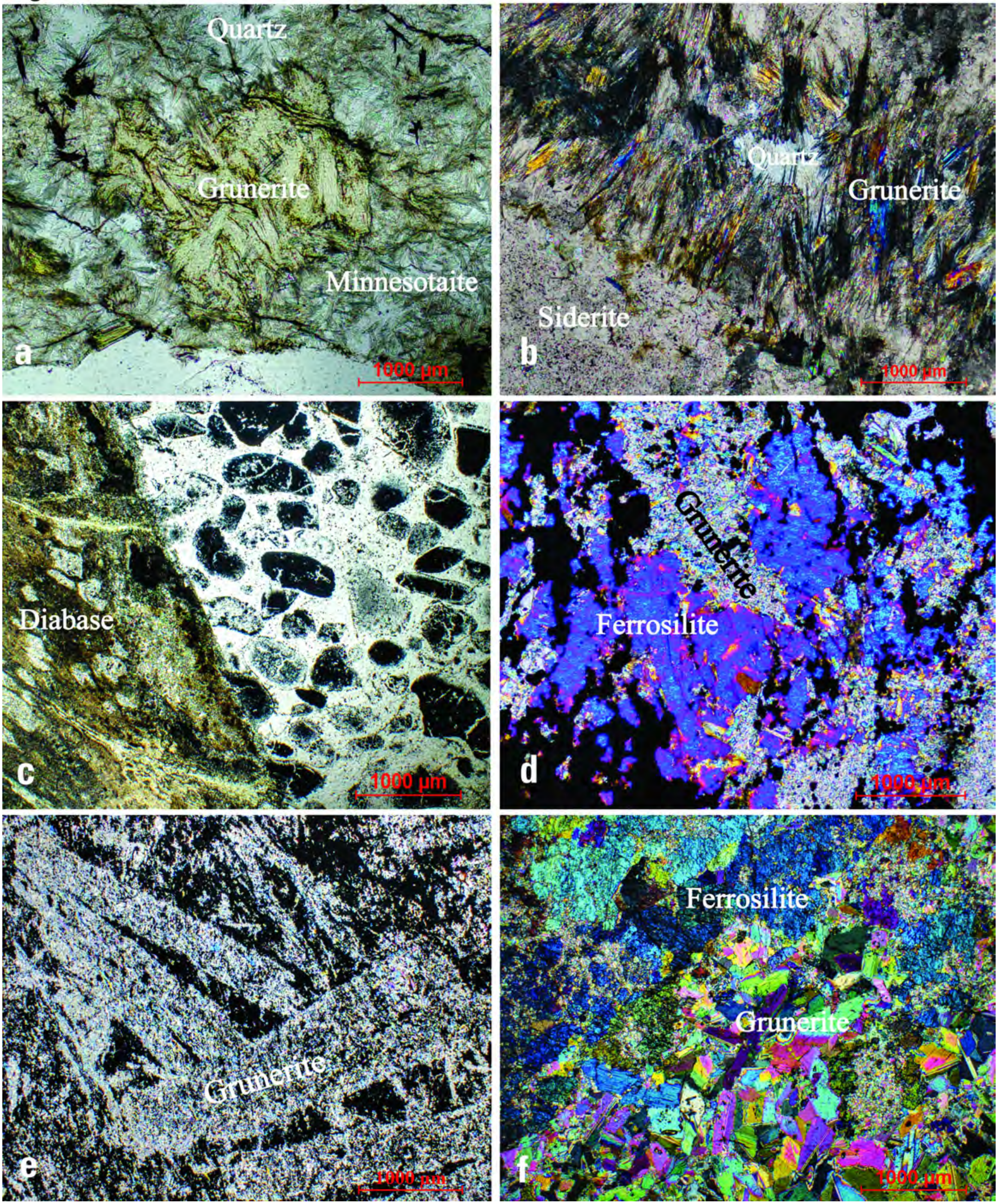

Figure 3

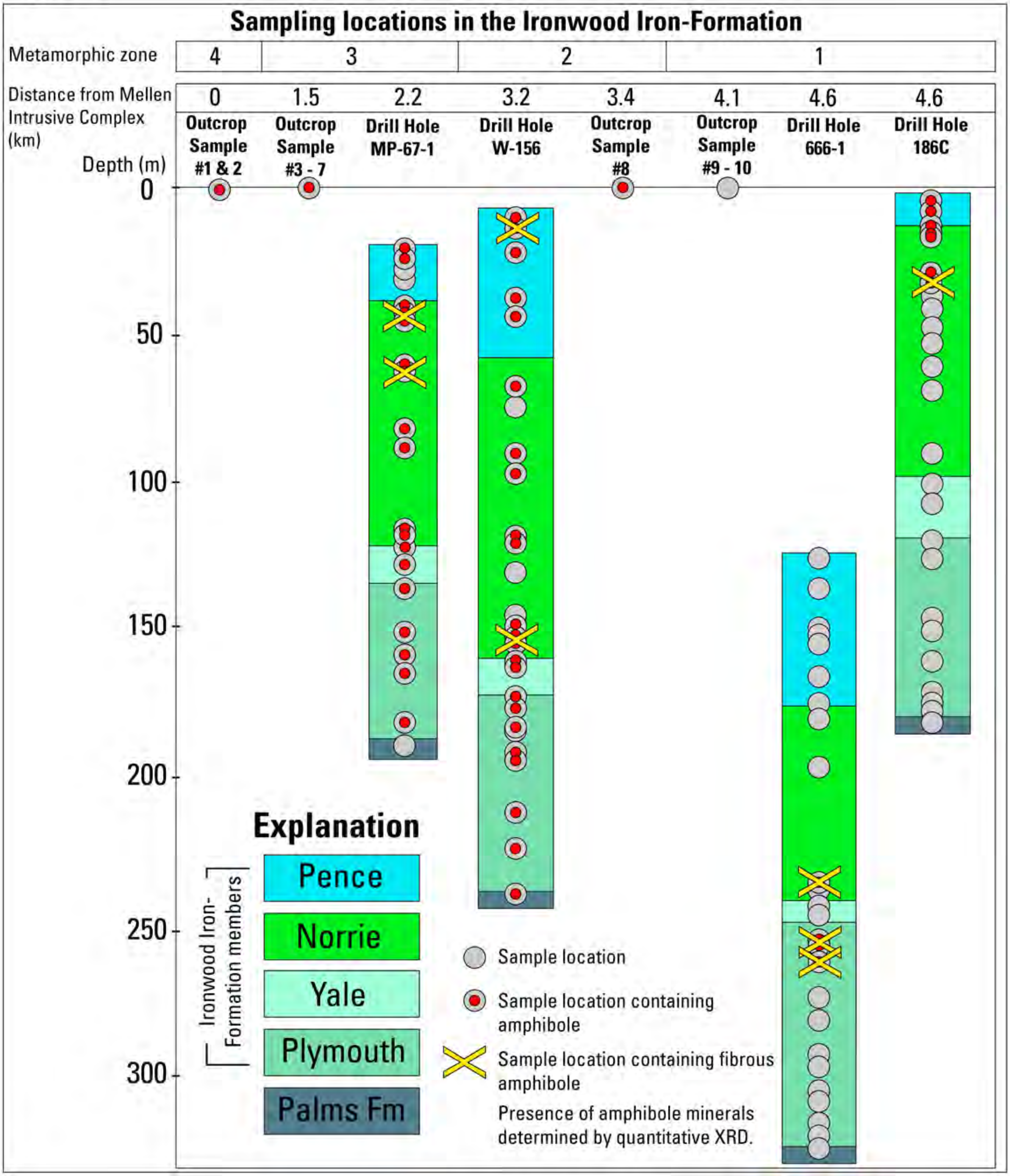
Sampling locations in the Ironwood Iron-Formation
Metamorphic zone
4
3
2
1
Distance from Mellen Intrusive Complex (km)
0
1.5
2.2
3.2
3.4
4.1
4.6
4.6
Outcrop Sample #1 & 2
Outcrop Sample #3 - 7
Drill Hole MP-67-1
Drill Hole W-156
Outcrop Sample #8
Outcrop Sample #9 - 10
Drill Hole 666-1
Drill Hole 186C
Depth (m)
0
50
100
150
200
250
300
Explanation
Ironwood Iron-Formation members
Pence
Norrie
Yale
Plymouth
Palms Fm
Sample location
Sample location containing amphibole
Sample location containing fibrous amphibole
Presence of amphibole minerals determined by quantitative XRD.

This is a preprint, the final version is subject to change, of the American Mineralogist (MSA)
Cite as Authors (Year) Title. American Mineralogist, in press.
DOI: https://doi.org/10.2138/am-2020-7211

Figure 4

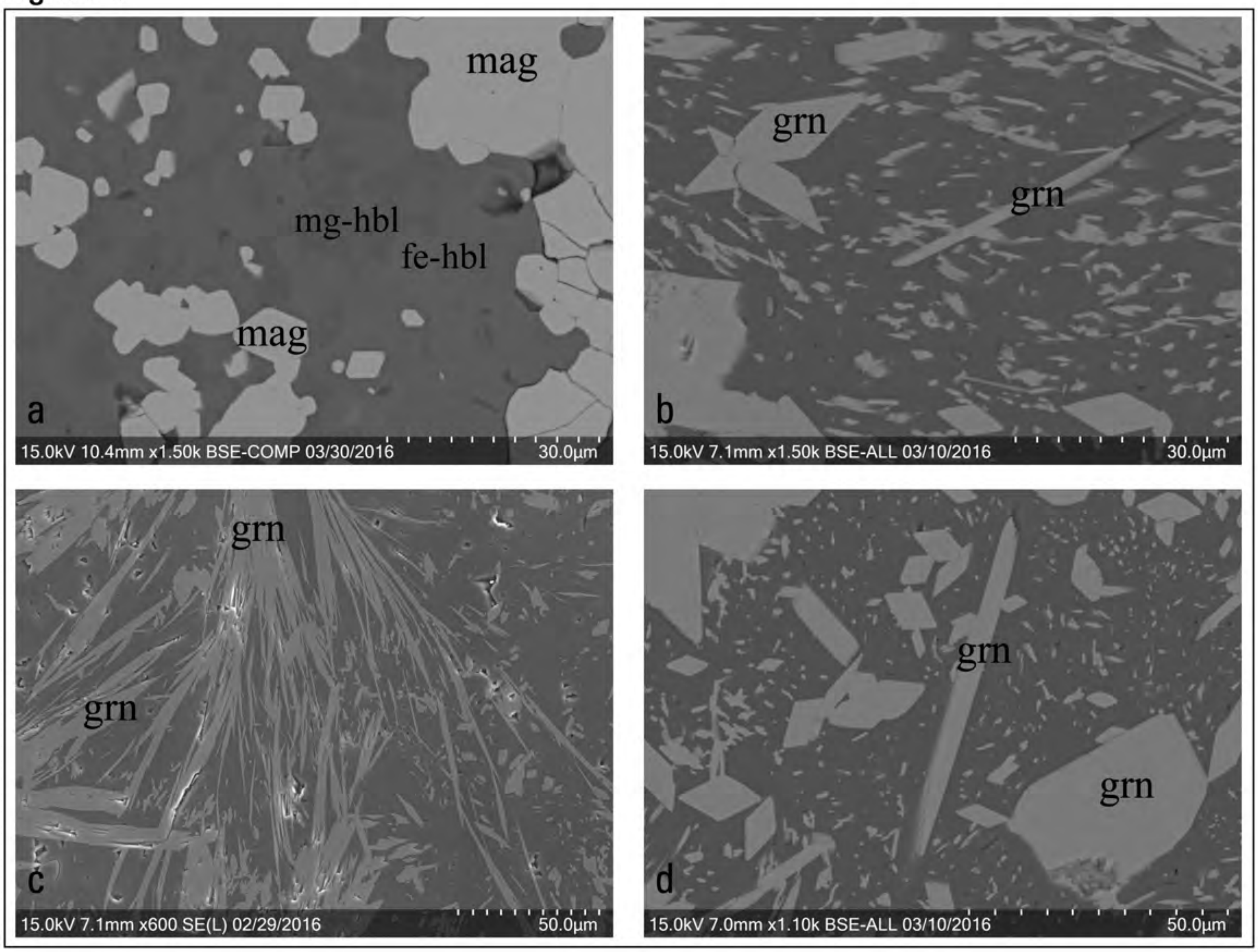

This is a preprint, the final version is subject to change, of the American Mineralogist (MSA)
Cite as Authors (Year) Title. American Mineralogist, in press.
DOI: https://doi.org/10.2138/am-2020-7211

Figure 5

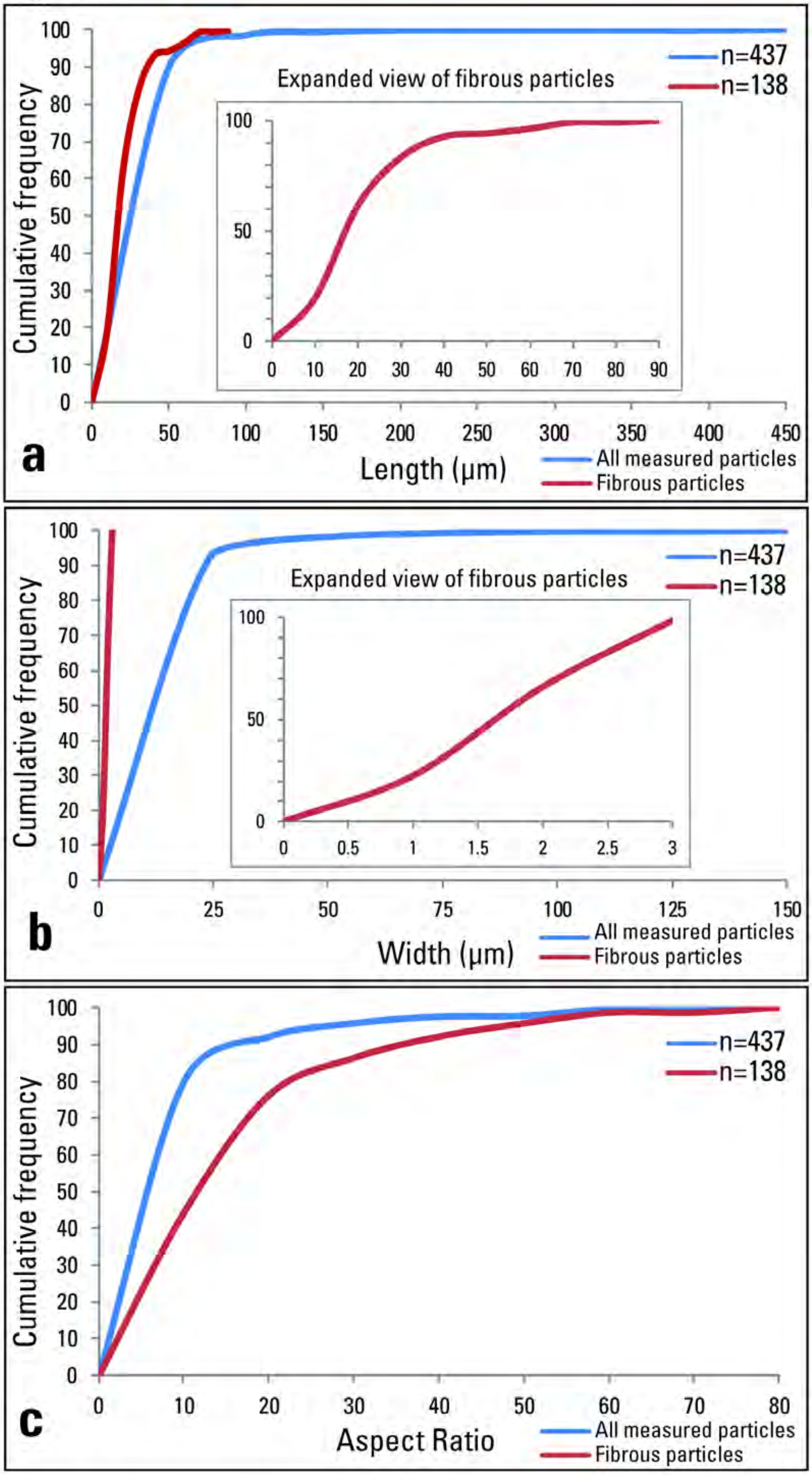

Figure 6

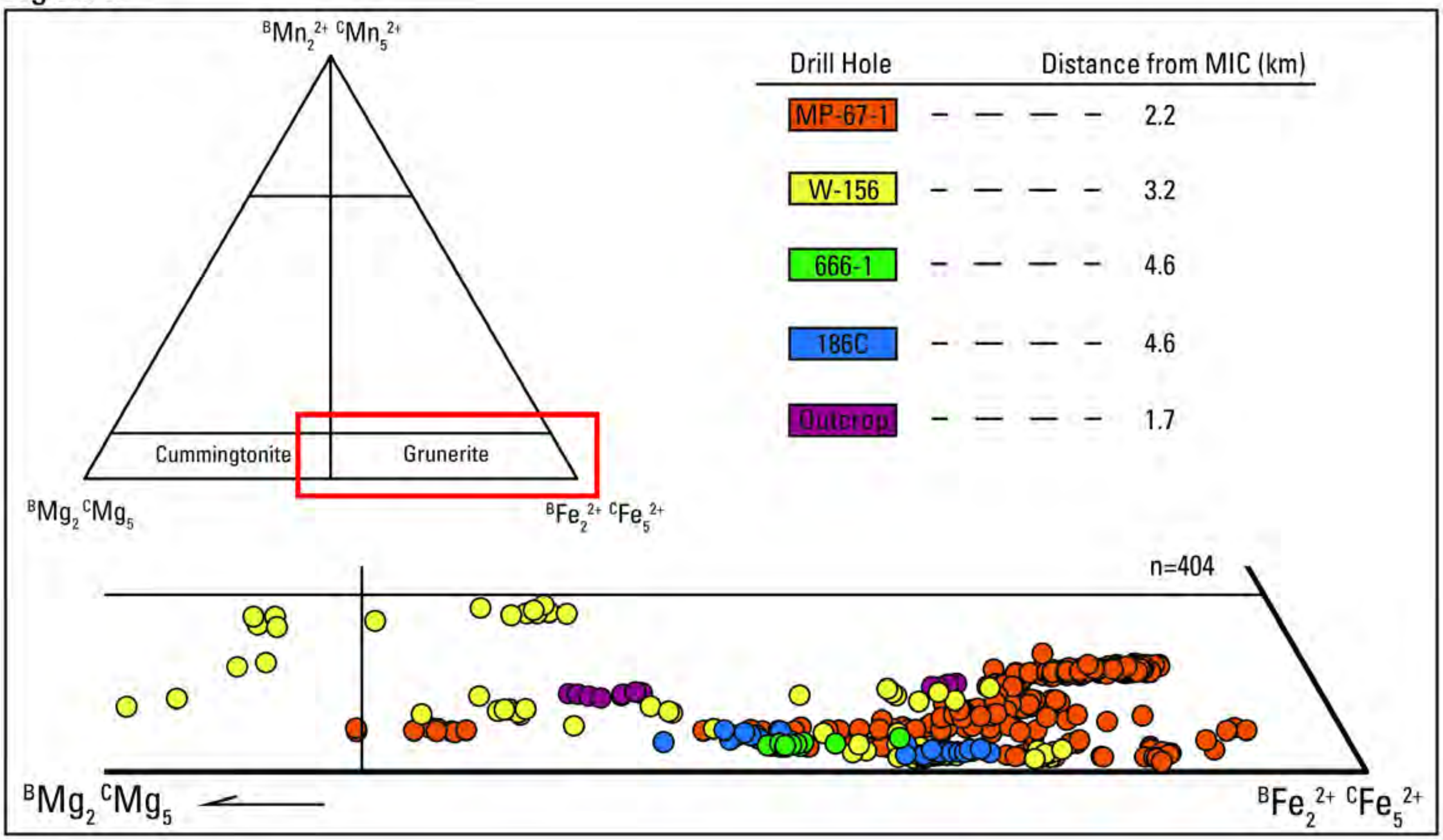

$^{B}Mn_2^{2+}$ $^{C}Mn_5^{2+}$
Cummingtonite
Grunerite
$^{B}Mg_2$ $^{C}Mg_5$
$^{B}Fe_2^{2+}$ $^{C}Fe_5^{2+}$
Drill Hole
Distance from MIC (km)
MP-67-1 2.2
W-156 3.2
666-1 4.6
186C 4.6
Outcrop 1.7
n=404
$^{B}Mg_2$ $^{C}Mg_5$
$^{B}Fe_2^{2+}$ $^{C}Fe_5^{2+}$

This is a preprint, the final version is subject to change, of the American Mineralogist (MSA)
Cite as Authors (Year) Title. American Mineralogist, in press.
DOI: https://doi.org/10.2138/am-2020-7211

Figure 7

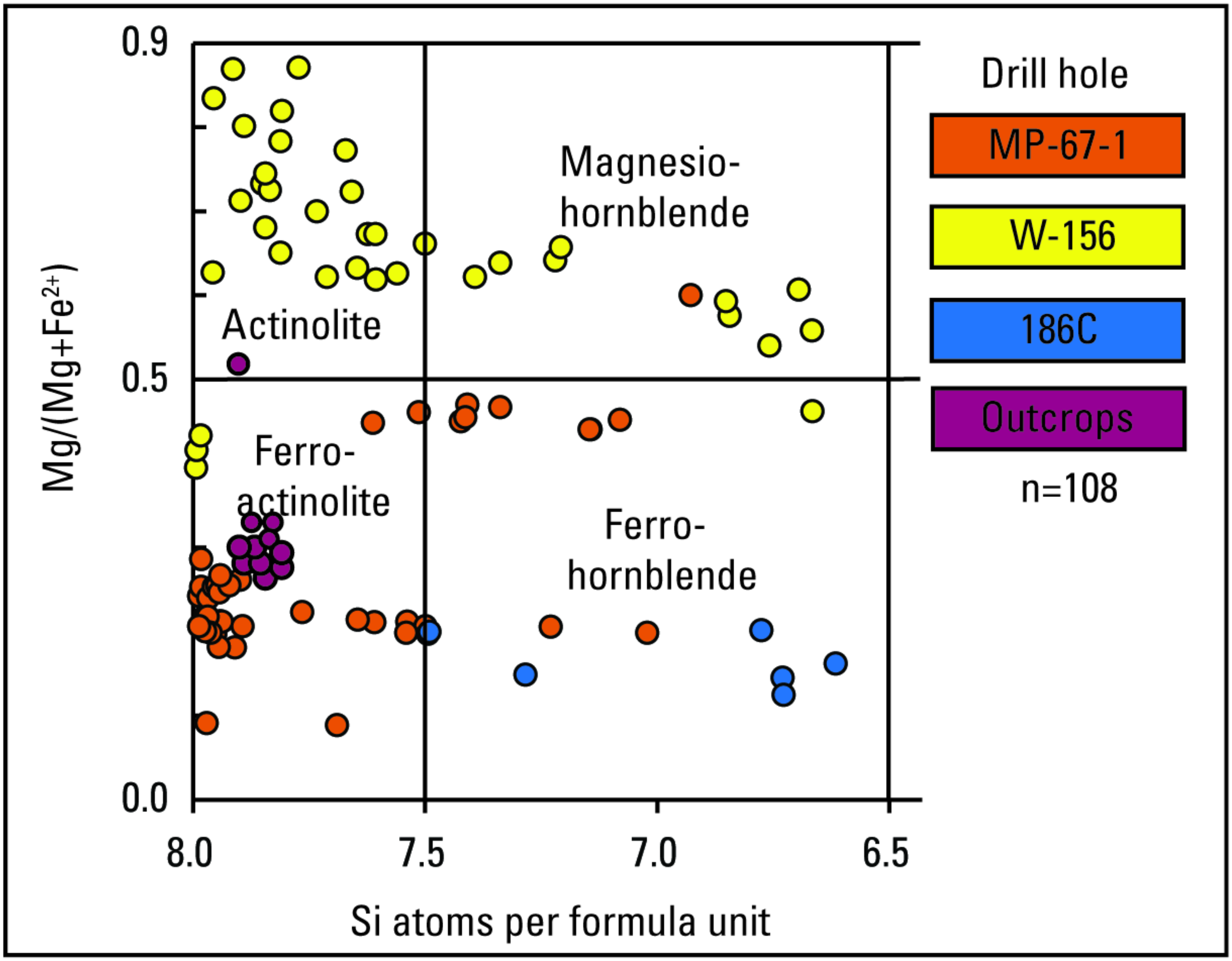

This is a preprint, the final version is subject to change, of the American Mineralogist (MSA)
Cite as Authors (Year) Title. American Mineralogist, in press.
DOI: https://doi.org/10.2138/am-2020-7211

Figure 8

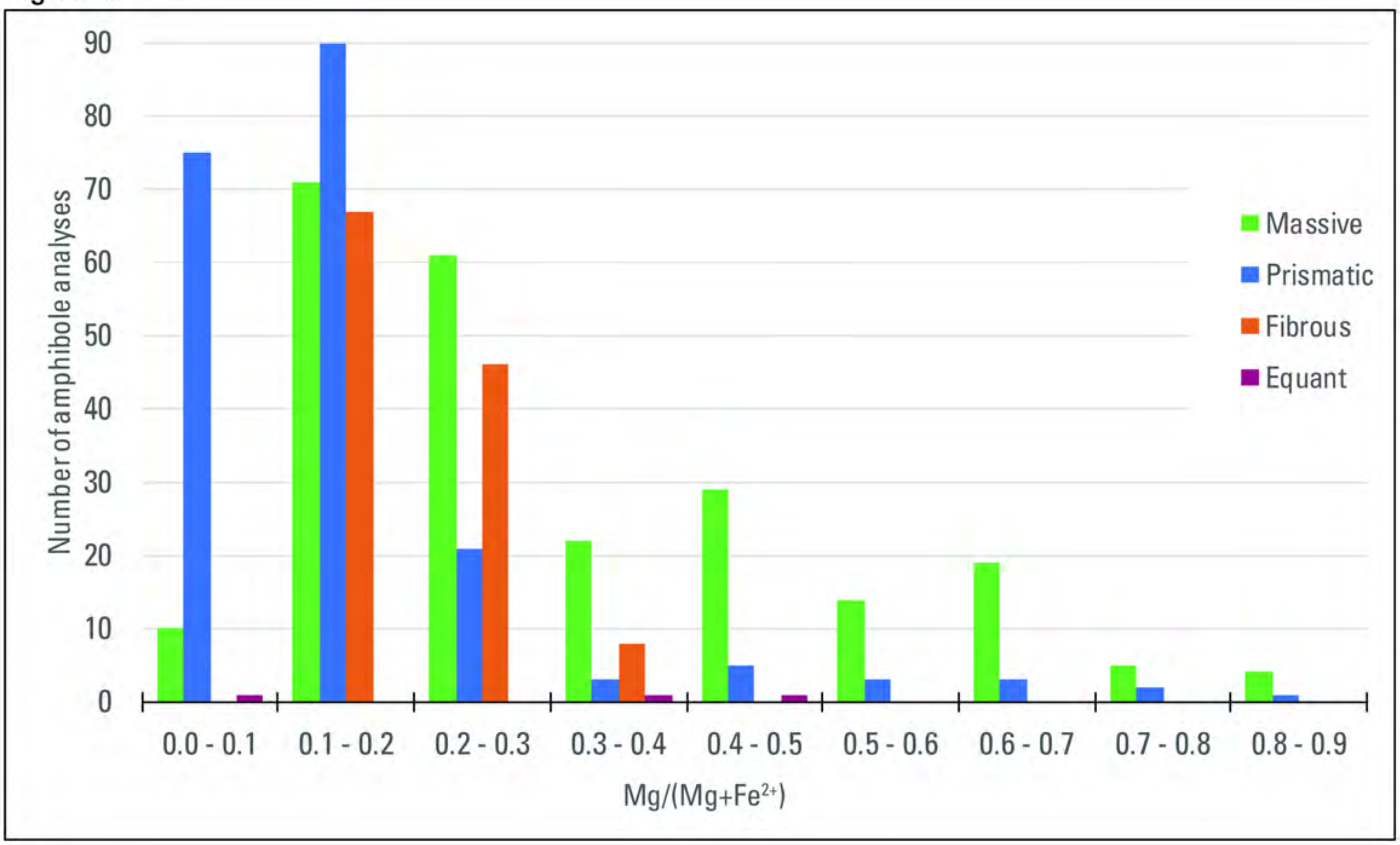

This is a preprint, the final version is subject to change, of the American Mineralogist (MSA)
Cite as Authors (Year) Title. American Mineralogist, in press.
DOI: https://doi.org/10.2138/am-2020-7211

Figure 9

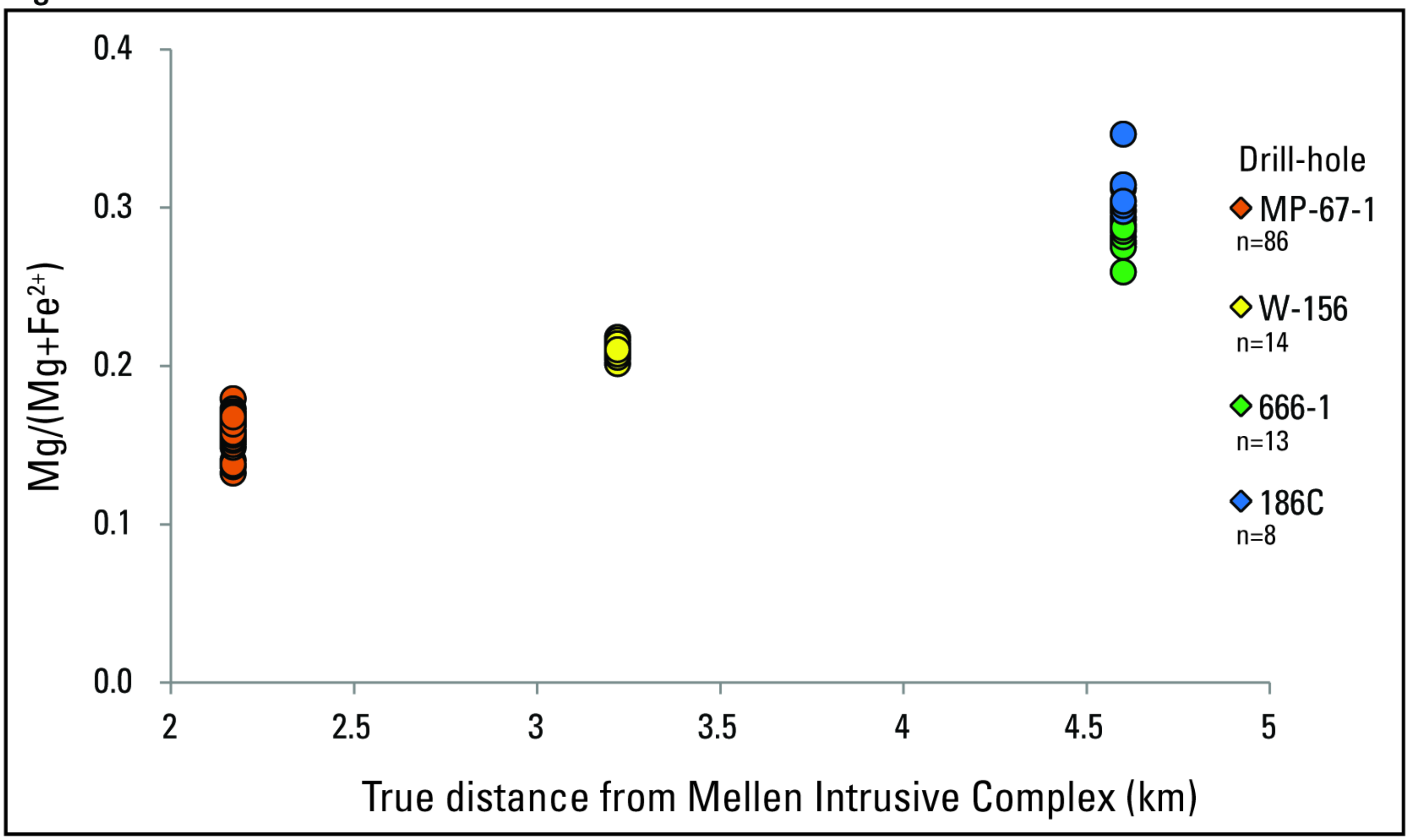

This is a preprint, the final version is subject to change, of the American Mineralogist (MSA)
Cite as Authors (Year) Title. American Mineralogist, in press.
DOI: https://doi.org/10.2138/am-2020-7211

Figure 10